Calculation of the magnetic surface function gradient in stellarators with broken stellarator symmetry

V. V. Nemov,[1,2] S. V. Kasilov,[1,2] W. Kernbichler,[2] and B. Seiwald[2]
[1]*Institute of Plasma Physics, National Science Center, Kharkov Institute of Physics and Technology, Akademicheskaya Str. 1, Kharkov 61108, Ukraine*
[2]*Association EURATOM-ÖAW, Institut für Theoretische Physik-Computational Physics, Technische Universität Graz, Petersgasse 16, Graz A-8010, Austria*

(Received 3 December 2009; accepted 24 March 2010; published online 27 May 2010)

The computation of the gradient of the magnetic surface function, $\nabla\psi$, plays an essential role in plasma physics, e.g., for investigations of plasma equilibrium currents or transport fluxes in stellarators. The evaluation of $\nabla\psi$ becomes more complicated if the magnetic field **B** does not exhibit stellarator symmetry. Here, a scheme for computation of $\nabla\psi$ for magnetic configurations which do not show stellarator symmetry is presented. The proposed method is based on computations of gradients of integrals of magnetic field line equations. This new technique for $\nabla\psi$ calculations is applied to Uragan-2M [O. S. Pavlichenko for the U-2M group, Plasma Phys. Controlled Fusion **35**, B223 (1993)]. Taking into account the influence of current feeds and detachable joints of the helical winding the magnetic configuration does not exhibit stellarator symmetry. Computations of $\nabla\psi$, the effective ripple ϵ_{eff}, and the geometrical factor λ_b for the bootstrap current in the $1/\nu$ transport regime are performed. © *2010 American Institute of Physics*. [doi:10.1063/1.3396366]

I. INTRODUCTION

For theoretical and numerical studies of various questions related to plasma confinement in toroidal systems it is necessary to calculate the gradient of the magnetic surface (flux surface) function,[1–5] $\nabla\psi$. In a toroidal plasma the equilibrium currents, transport fluxes and other quantities are expressed trough this gradient. For calculation of $\nabla\psi$ for the realistic magnetic field, **B**, of a toroidal device given in real-space coordinates numerical methods are necessary if the magnetic field does not exhibit any kind of symmetry and if there is no simplification in the magnetic field representation. A convenient technique for the $\nabla\psi$ computation under such conditions has been presented in Ref. 6.

The technique presented in Ref. 6 is based on integration along magnetic field lines. The quantity $\nabla\psi$ is considered as a gradient of one of the integrals of the magnetic field line equations and is calculated using the corresponding differential equations for $\nabla\psi$. This technique has been applied in a number of papers related to studies of plasma equilibrium currents and neoclassical transport for stellarator type magnetic fields which are originally available in real-space coordinates (see, e.g., in Refs. 7–9). In most of the configurations treated in these references the magnetic fields possess the so-called stellarator symmetry. Such a symmetry manifests itself in existence of magnetic surface cross sections with "up-down" symmetry. This simplifies the problem of determining initial conditions for integrating the $\nabla\psi$ equations. The determination of these conditions is significantly more complicated if the stellarator symmetry is violated. In such a case, a preliminary computation of the corresponding magnetic surface is necessary in order to find these initial conditions.

In this paper, an effective technique for computing $\nabla\psi$ and associated quantities for stellarator magnetic fields with violated stellarator symmetry is introduced. To evaluate $\nabla\psi$ the gradients of two integrals of the magnetic field line equations are determined.

This paper is organized as follows. Section II describes the derivation of equations and formulas for computation of $\nabla\psi$. In Sec. III a model of the magnetic field with broken stellarator symmetry is discussed, namely, the magnetic field of the Uragan-2M (U-2M) torsatron.[10] For this magnetic configuration the influence of current feeds and detachable joints of the helical winding is taken into account. Computations of $\nabla\psi$, the effective ripple ϵ_{eff}, and equilibrium currents are performed in Sec. IV. The geometrical factor for the bootstrap current in the $1/\nu$ transport regime, which is often characteristic for stellarators, is also computed. Some conclusions are presented in Sec. V.

II. BASIC EQUATIONS

It is well known that in an arbitrary toroidal magnetic field one can always find two independent integrals of the equations of the magnetic field lines (see, e.g., Ref. 3). If magnetic surfaces (regular or island surfaces) exist, one of these integrals can be found as a single valued integral ψ, the magnetic surface integral. With this, another independent integral, θ, turns out to be not single valued and $\nabla\theta$ increases in general continuously along the magnetic field line (in case of $d\iota/d\psi \neq 0$ where ι is the rotational transform).

In general there exists an infinite set of integrals of magnetic field line equations. Each of those integrals can be represented as some function of the two above mentioned independent integrals. And, vice versa, the magnetic surface integral ψ can be expressed as a function of two independent

integrals. Consequently, the evolution of $\nabla\psi$ along the magnetic field line can be expressed as a linear combination of gradients of these two independent integrals,

$$\nabla\psi = \nabla\theta_1 + \alpha\nabla\theta_2, \tag{1}$$

with $\nabla\theta_1$ and $\nabla\theta_2$ being gradients of conveniently chosen independent not single valued integrals of the magnetic field line equations. To evaluate $\nabla\theta_1$ and $\nabla\theta_2$ the equations

$$\frac{dQ_{1,i}}{ds} = -\frac{1}{B}\frac{\partial B^j}{\partial \xi^i}Q_{1,j}, \tag{2}$$

$$\frac{dQ_{2,i}}{ds} = -\frac{1}{B}\frac{\partial B^j}{\partial \xi^i}Q_{2,j}, \tag{3}$$

can be used. Here, s is the distance along the field line, B^j are the contravariant components of $\mathbf{B}$ in real space coordinates ξ^i, whereas $Q_{1,j}=\partial\theta_1/\partial\xi^j$ and $Q_{2,j}=\partial\theta_2/\partial\xi^j$ are the covariant components of $\mathbf{Q_1}\equiv\nabla\theta_1$ and $\mathbf{Q_2}\equiv\nabla\theta_2$, respectively. Equations (2) and (3) are a consequence of the equation $\mathbf{B}\cdot\nabla\theta_{1,2}=0$ (see Ref. 6).

To determine $\nabla\psi$ with help of Eq. (1), the quantity α has to be found. Preliminary computations of any magnetic surfaces have to be achieved. The integration of the magnetic field line that determines the magnetic surface as well as the integration of Eqs. (2) and (3) have to be performed for a sufficiently large integration interval corresponding to a sufficiently large number of turns around the torus. During this integration all intersections of the field line with the initial cross section of the magnetic surface are monitored. The intersection, which is nearest to the initial point of the integration $\mathbf{r}_{st}$, is chosen as the final integration point $\mathbf{r}_{fin}$. Since $\mathbf{r}_{fin}$ is close to $\mathbf{r}_{st}$, the quantities $\nabla\psi_{st}$ and $\nabla\psi_{fin}$ should also be close to each other. Here, $\nabla\psi_{st}$ and $\nabla\psi_{fin}$ are the magnetic surface gradients $\nabla\psi$ at $\mathbf{r}_{st}$ and $\mathbf{r}_{fin}$, respectively. Therefore, the quantity $f(\alpha)=(\nabla\psi_{fin}-\nabla\psi_{st})^2$, or

$$f(\alpha) = (\nabla\theta_{1,fin} + \alpha\nabla\theta_{2,fin} - \nabla\theta_{1,st} - \alpha\nabla\theta_{2,st})^2, \tag{4}$$

should be small. To find α one has to minimize $f(\alpha)$. Equating the derivative of $f(\alpha)$ with respect to α to zero, one finds

$$\alpha = -\frac{b}{a}, \tag{5}$$

with

$$a = (\nabla\theta_{2,fin} - \nabla\theta_{2,st})^2,$$
$$b = (\nabla\theta_{1,fin} - \nabla\theta_{1,st})\cdot(\nabla\theta_{2,fin} - \nabla\theta_{2,st}). \tag{6}$$

It has to be ensured that the quantity α is determined with high accuracy. In the next step, $\nabla\psi$ and associated quantities can be computed. In particular $\nabla\psi_{st}$ can be found using formula (1) for $\nabla\theta_1=\nabla\theta_{1,st}$ and $\nabla\theta_2=\nabla\theta_{2,st}$. After that the approach of Ref. 6 can be used for further calculation of $\nabla\psi$. In this case instead of two sets of Eqs. (2) and (3) only one set of equations of type (2) or (3) can be solved directly for the vector $\mathbf{P}\equiv\nabla\psi$:

$$\frac{dP_i}{ds} = -\frac{1}{B}\frac{\partial B^j}{\partial \xi^i}P_j,$$

with $P_j=\partial\psi/\partial\xi^j$ [see also Eq. (55) in Ref. 8]. Comparing the total computer time expenses it can be seen that the evaluation of $\nabla\psi$ for magnetic configurations with lack of stellarator symmetry is much more time consuming than the computation of $\nabla\psi$ for magnetic configuration exhibiting stellarator symmetry.

III. MAGNETIC FIELD PARAMETERS

To demonstrate the capabilities of the proposed approach computations are performed for the magnetic configuration of U-2M ($l=2$ torsatron, major radius $R=170$ cm, number of helical field periods along the torus $n_p=4$; see Ref. 10). The influences of current-feeds and detachable joints of the helical winding are taken into account. Because of the nonsymmetric arrangement of these elements of the magnetic system, the stellarator symmetry of the resulting magnetic field of U-2M is violated and there exists no cross section of magnetic surfaces with an up-down symmetry. The resulting magnetic field and its spatial derivatives can be computed using the Biot–Savart code of Ref. 11. This code is a refinement of the former code of Refs. 12 and 13 in which computations of magnetic surfaces for U-2M have been performed taking into account the current feeds and detachable joints.

In addition to Biot–Savart computations, the validity of the $\nabla\psi$ computation is checked by representing the magnetic field as the superposition of a finite number of toroidal harmonic functions containing the associated Legendre functions to minimize the computer time expenses. The form of the superposition given in Ref. 14 is used:

$$\mathbf{B} = \nabla\Phi + \nabla\times\mathbf{A}_\varphi + \mathbf{e}_\varphi b_0 R/\rho, \tag{7}$$

$$\Phi = \sum_{n=0}^{\infty}\sum_{\substack{m=-\infty \\ (m\neq 0)}}^{\infty} H_{nmc}\Phi_{nmc} + H_{nms}\Phi_{nms}, \tag{8}$$

$$\Phi_{nms} = \sqrt{\cosh\,\eta - \cos\,\theta}\,Q^m_{n-1/2}(\cosh\,\eta)\sin(n\theta + m\varphi), \tag{9}$$

$$\Phi_{nmc} = \sqrt{\cosh\,\eta - \cos\,\theta}\,Q^m_{n-1/2}(\cosh\,\eta)\cos(n\theta + m\varphi), \tag{10}$$

$$A_\varphi = \sum_{n=0}^{\infty} C_{nc}A_{\varphi nc} + C_{ns}A_{\varphi ns}, \tag{11}$$

$$A_{\varphi ns} = \sqrt{\cosh\,\eta - \cos\,\theta}\,Q^1_{n-1/2}(\cosh\,\eta)\sin(n\theta), \tag{12}$$

$$A_{\varphi nc} = \sqrt{\cosh\,\eta - \cos\,\theta}\,Q^1_{n-1/2}(\cosh\,\eta)\cos(n\theta). \tag{13}$$

Here, Φ and $\mathbf{A}_\varphi$ are the scalar and vector potentials, respectively, $Q^m_{n-1/2}$ are associated Legendre functions of the second kind, (η,θ,φ) is the toroidal system of coordinates associated with the cylindrical system (ρ,φ,z), n and m are the poloidal and toroidal harmonic numbers, R is the major ra-

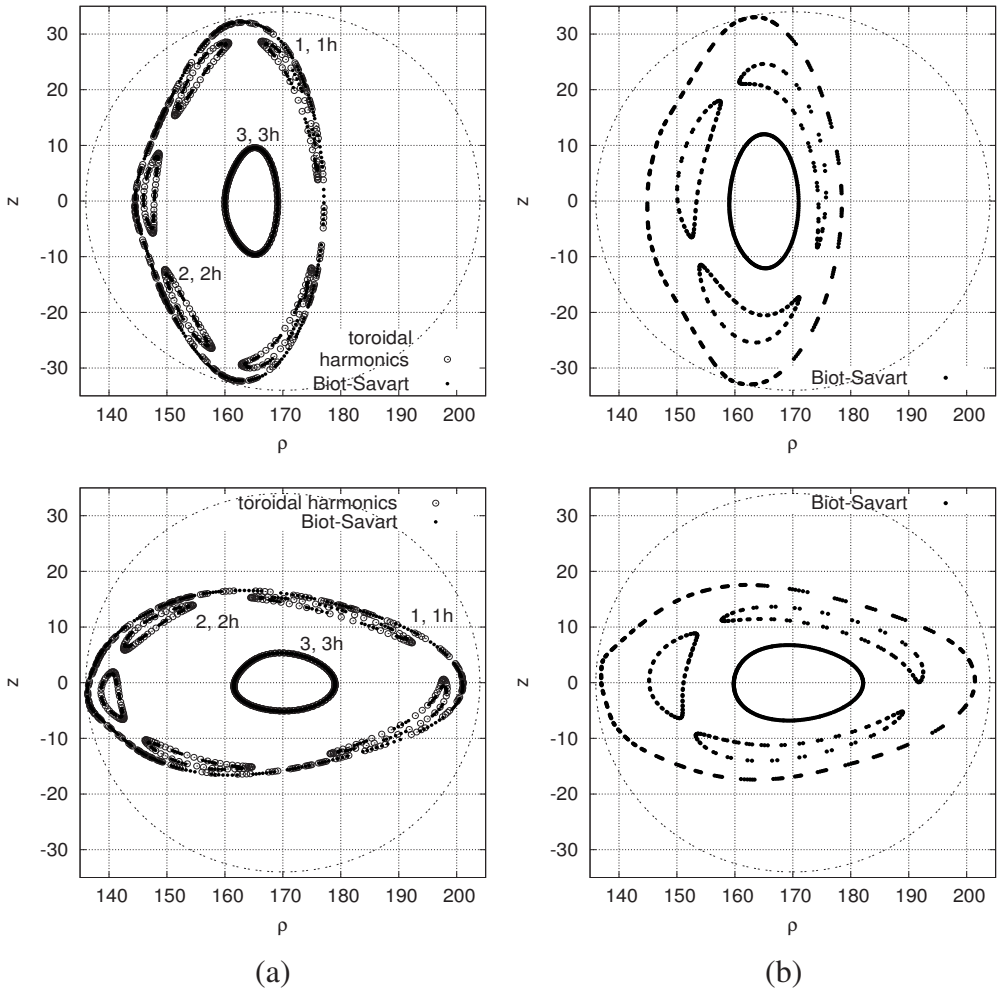

FIG. 1. (a) Magnetic surfaces of U-2M (k_φ=0.31) inside the vacuum chamber for φ=0 (top) and φ=$-\pi/4$ (bottom). The circle with a radius of 34 cm represents the inner boundary of the vacuum chamber. The curves 1, 2, and 3 (dots; ι=0.4244, 2/5, and 0.3384, respectively) correspond to the Biot–Savart computations, curves 1h, 2h, and 3h (open circles, ι=0.426, 2/5, and 0.3382, respectively) correspond to modeling the field with toroidal harmonics. The integration has been started for the curves 1 and 1h at R_{st}=144.5 cm (in the φ=0 plane), for 2 and 2h at R_{st}=147.8 cm, and for 3 and 3h at R_{st}=160.0 cm. (b) Inner, island (ι=1/3), and boundary magnetic surfaces of U-2M in case of k_φ=0.295 for φ=0 and φ=$-\pi/4$.

dius of the torus, and H_{nms}, H_{nmc}, C_{ns}, and C_{nc} are the expansion coefficients.

The expansion coefficients of the decomposition are obtained with preliminary computations of the magnetic field using the Biot–Savart code. A total number of 158 toroidal harmonics is used for the presented computations. Note that a representation of the magnetic field is necessary where sine as well as cosine harmonics are taken into account in the scalar and vector potentials in order to describe the properties of the magnetic field without stellarator symmetry. If the magnetic field exhibits stellarator symmetry, it is sufficient to use only sine terms in the scalar potential and cosine terms in the vector potential (see, e.g., in Ref. 8).

For the study two different vacuum magnetic configurations of U-2M are considered. For both configurations magnetic field parameters are chosen to provide magnetic surfaces which are well centered with respect to the vacuum chamber. For the first configuration the toroidal magnetic field is chosen in such a way that the rotational transform ι is within $1/3<\iota<1/2$ [k_φ=0.31, see, in Refs. 10, 11, and 13, $k_\varphi=B_{th}/(B_{th}+B_{tt})$, where B_{th} and B_{tt} are the toroidal components of the magnetic field produced by the helical winding and the toroidal field coils, respectively]. The second configuration (k_φ=0.295, see Ref. 10) has a slightly larger toroidal magnetic field and ι is within $0.31<\iota<0.383$. For this configuration the island magnetic surfaces with ι=1/3 are inside the confinement region.

To demonstrate the accuracy of the magnetic field representation with help of toroidal harmonics, cross sections of the magnetic surfaces are compared. The **B**-field is computed using both the representation with toroidal harmonics as well as the Biot–Savart law. For this purpose the magnetic configuration characterized by k_φ=0.31 is used. The result of this comparison is presented in Fig. 1(a) for magnetic surfaces corresponding to three starting points for the integration, R_{st}, in the φ=0 plane (z=0). It follows from the figure that for the magnetic field representation with toroidal harmonics the shapes of the magnetic surfaces as well as the rotational transform are in good agreement with those obtained from the Biot–Savart code. Also, some magnetic surfaces obtained with help of the Biot–Savart code are shown

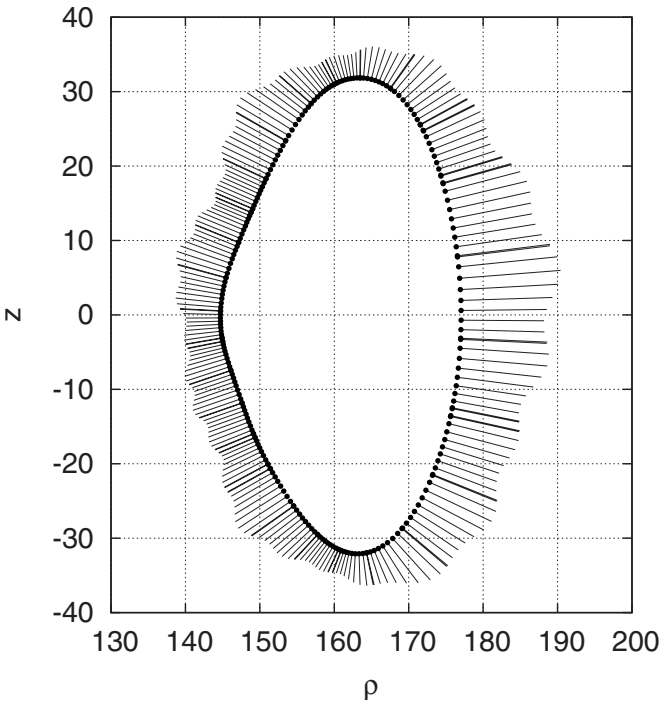

FIG. 2. The magnetic surface, with starting point for the integration $R_{st}=144.7$ cm ($\iota=0.423$), and its magnetic surface gradient $\nabla\psi$ in the $\varphi=0$ plane ($k_\varphi=0.31$, magnetic field is represented with help of toroidal harmonics).

in Fig. 1(b) for the case of $k_\varphi=0.295$ to characterize this magnetic configuration.

IV. CALCULATION OF $\nabla\psi$, EQUILIBRIUM CURRENTS, AND THE $1/\nu$ NEOCLASSICAL TRANSPORT

To determine the parameter α [see Eq. (5)] in preliminary computations for any starting point $\mathbf{r_{st}}$, the magnetic field line as well as Eqs. (2) and (3) have been integrated for an interval corresponding to 250 or 500 turns around the z axis in the cylindrical coordinates ρ,φ,z. For the integration of Eqs. (2) and (3) the following quantities are used as initial values of $\nabla\theta_1$ and $\nabla\theta_2$, $\nabla\theta_{1,st}$ and $\nabla\theta_{2,st}$, respectively:

$$\nabla\theta_{1,st}=\mathbf{B}\times\mathbf{e}_z/B, \tag{14}$$

$$\nabla\theta_{2,st}=\mathbf{B}\times\mathbf{e}_\rho/B, \tag{15}$$

with $\mathbf{e}_\rho$ and $\mathbf{e}_z$ being the basis vectors (physical) of the cylindrical coordinate system. Once α has been computed, $\nabla\psi$, given in Eq. (1), and associated quantities can be calculated.

A. Calculation of $\nabla\psi$ and the Pfirsch–Schlüter currents

Having calculated $\nabla\psi$, the equilibrium plasma current densities $j_\parallel$ and $j_\perp$, which are determined by the plasma pressure gradient, can be calculated from equations (see, e.g., in Refs. 2, 5, and 7),

$$\mathbf{j}_\perp=c\frac{dp}{d\psi}\frac{\mathbf{B}\times\nabla\psi}{B^2}, \tag{16}$$

$$\mathbf{j}_\parallel=-c\frac{dp}{d\psi}h\mathbf{B}, \tag{17}$$

$$\frac{dh}{ds}=2\frac{|\nabla\psi|k_G}{B^2}, \tag{18}$$

with the plasma pressure $p=p(\psi)$, the geodesic curvature k_G of a magnetic field line, and

$$|\nabla\psi|k_G=\frac{\mathbf{B}\times\nabla B\cdot\nabla\psi}{B^2}. \tag{19}$$

Equation (18) is obtained from the magnetic differential equation

$$\mathbf{B}\cdot\nabla h=2\frac{|\nabla\psi|k_G}{B}. \tag{20}$$

The solution of Eq. (17) which corresponds to the zero net toroidal current condition[2,4] results in the so called Pfirsch–Schlüter current, j_{ps}. The quantity μ, which is connected to $j_\parallel$ and $j_\perp$,

$$\mu=\frac{1}{2}\frac{j_\parallel}{j_\perp}, \tag{21}$$

is of interest since it is independent of the plasma pressure gradient and characterizes the magnetic field geometry. A decrease in $j_\parallel/j_\perp$ (see, e.g., in Ref. 15) corresponds to a decrease in the perturbation of the vacuum magnetic configuration caused by a plasma with finite β (β is the ratio of the gas kinetic pressure to the magnetic pressure).

The results of this subsection relate to the U-2M magnetic configuration with $k_\varphi=0.31$. The magnetic field is represented with help of toroidal harmonics. Figure 2 shows the results of the $\nabla\psi$ computation for a magnetic surface with starting point for the field line integration at $R_{st}=144.7$ cm ($z_{st}=0$, $\varphi=0$, $\iota=0.423$). The puncture plot for the magnetic surface cross section is presented in the $\varphi=0$ plane. The segments of solid lines show the projection of $\nabla\psi$ (in a convenient scale) onto the $\varphi=$const plane. A single valued character of the $\nabla\psi$ distribution is evident.

The results for the Pfirsch–Schlüter current calculations for the same magnetic surface as used for Fig. 2 are presented in Fig. 3. For the $\varphi=0$ and $\varphi=-\pi/4$ cross sections the parameter μ is presented as a function of $\vartheta/2\pi$, with ϑ being the poloidal angle counted from the direction of the normal to the circular axis of the torus. Note that for the magnetic field of a conventional stellarator with circular cross sections of magnetic surfaces the analogous distribution of μ is of cosine form with an amplitude value of $1/\iota$.

For comparison, the parameter μ is calculated also with a different technique for evaluating $\nabla\psi$. According to Ref. 16 (see also in Ref. 11), $\nabla\psi$ can be represented in cylindrical coordinates as

$$\nabla\psi=\lim_{\mathbf{r}_2(\varphi_0)\to\mathbf{r}_1(\varphi_0)}\frac{[\mathbf{r}_2(\varphi)-\mathbf{r}_1(\varphi)]\times\mathbf{B}}{|[\mathbf{r}_2(\varphi_0)-\mathbf{r}_1(\varphi_0)]\times\mathbf{B}(\boldsymbol{\varphi_0})|}. \tag{22}$$

Here, the curves $\mathbf{r}_1(\varphi)$ and $\mathbf{r}_2(\varphi)$ satisfy the field line equations $d\mathbf{r}/d\varphi=\rho\mathbf{B}/B_\varphi$ with starting points $\mathbf{r}_1(\varphi_0)$ and $\mathbf{r}_2(\varphi_0)$, respectively, and $\mathbf{B}(\boldsymbol{\varphi_0})$ is $\mathbf{B}$ for the starting point $\mathbf{r}_1(\varphi_0)$. The

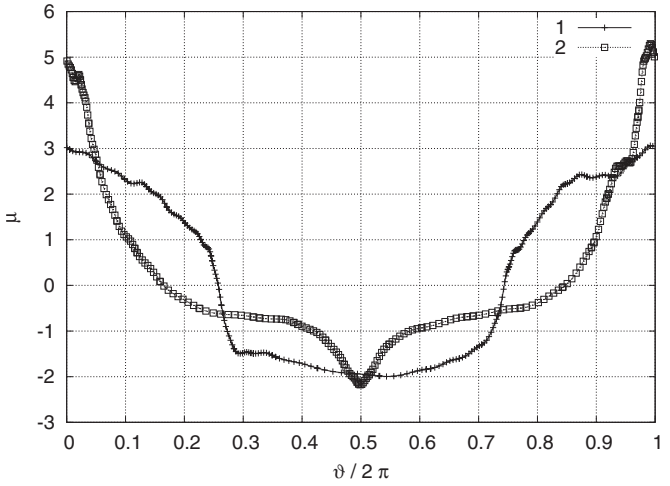

FIG. 3. The quantity $\mu=0.5j_{\|}/j_{\perp}$ [see also Eq. (21)] for the magnetic surface presented in Fig. 2, in the $\varphi=0$ (curve 1) and $\varphi=-\pi/4$ (curve 2) planes.

initial points $\mathbf{r}_1(\varphi_0)$ and $\mathbf{r}_2(\varphi_0)$ are on the same magnetic surface and on the same meridian plane φ_0. In the preliminary computation of any magnetic surface corresponding to the initial point $\mathbf{r}_1(\varphi_0)$, the second starting point $\mathbf{r}_2(\varphi_0)$ can be found in the same way as the point $\mathbf{r}_{fin}$ in Sec. II.

For the magnetic surface corresponding to $R_{st}=144.7$ cm the results of the $\nabla\psi$ computation using formula (22) are very close to those shown in Fig. 2. The results for the parameter μ are presented in Fig. 4. In contrast with Fig. 3 substantial irregularities are seen in the curves of Fig. 4. The reason is that in Eq. (22) the quantity $\mathbf{r}_2(\varphi)-\mathbf{r}_1(\varphi)$ is not infinitesimally small. In practice it is small but finite. A small inaccuracy in the $\nabla\psi$ calculation leads to a violation of the equality $\langle|\nabla\psi|k_G/B\rangle=0$ which is a condition of a single valued (see, e.g., Refs. 2 and 5) solution of the magnetic differential Eq. (20). Here, the angular brackets $\langle\cdots\rangle$ denote the average over the volume of a thin layer between neighboring magnetic surfaces. For nonrational magnetic surfaces (which are realized in stellarators in most cases) this average can be calculated using the integration along the magnetic field line applying the formula

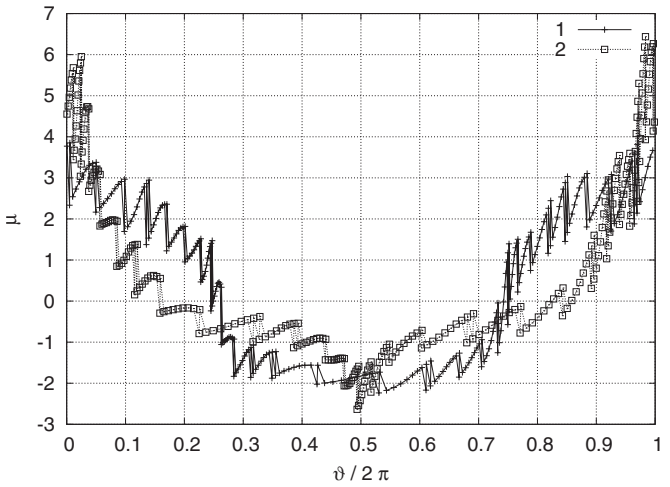

FIG. 4. The same as in Fig. 3, but using formula (22) for the $\nabla\psi$ calculation.

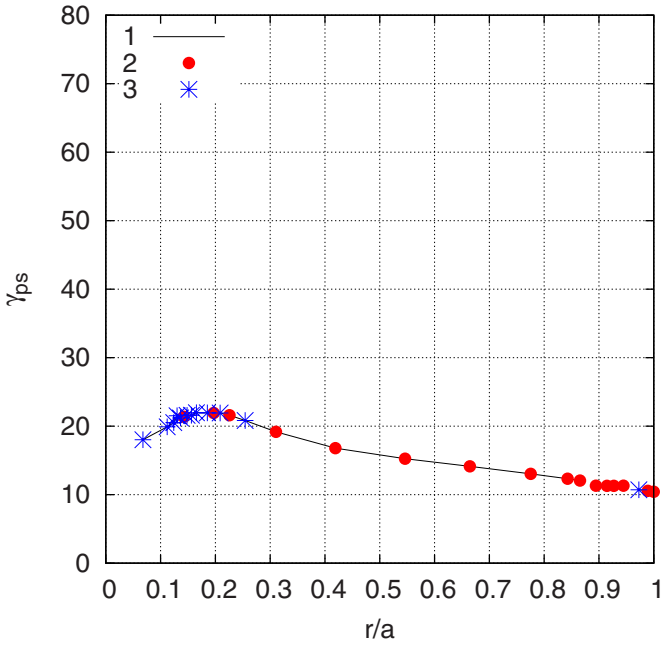

FIG. 5. (Color online) Computational results for the Pfirsch–Schlüter factor γ_{ps} (curve 1) using the Biot–Savart code for $k_{\varphi}=0.31$, 2: results for the cases of good convergence of solution for $j_{\|}$, 3: results for the cases of some violation of convergence of the $j_{\|}$ solution; r is a mean radius of the magnetic surface, a is a mean radius of the outermost magnetic surface inside the vacuum chamber. Values of γ_{ps} for $0.87<r/a<0.96$ correspond to island magnetic surfaces with $\iota=2/5$. The values of r/a for these points are shown schematically.

$$\langle A\rangle=\lim_{L\to\infty}\left(\int_0^L\frac{ds}{B}\right)^{-1}\int_0^L ds\frac{A}{B}. \tag{23}$$

So, a small nonzero constant component appears in the right hand side of Eq. (18). For large integration intervals this leads to growth of the value h and to irregularities in computational results for the $j_{\|}$ distribution. The obtained results demonstrate the advantages of the technique of $\nabla\psi$ calculation presented in Sec. II.

B. Pfirsch–Schlüter factor (secondary currents) study

The parameter μ, Eq. (21), represents a local value of the ratio of the parallel to the perpendicular current densities. Another important parameter connected with these currents is the so called Pfirsch–Schlüter factor,

$$\gamma_{ps}=\langle j_{\|}^2\rangle/\langle j_{\perp}^2\rangle. \tag{24}$$

The averaging in Eq. (24) is performed using the rule (23). Computations of $j_{\|}$ are performed with the usage of Eq. (17) under the condition of zero net toroidal current. Under this condition the secondary current $j_{\|}$ is the so called Pfirsch–Schlüter current, j_{ps}. Minimization of the ratio (24) is understood to be important for stellarator optimization since a reduction *of* j_{ps} improves the equilibrium conditions of the plasma (see, e.g., in Ref. 15). Computational results obtained for both configurations for the magnetic field computed using the Biot–Savart code are presented in Figs. 5 and 6.

For the tokamak or the classical stellarator γ_{ps} can be evaluated by the ratio $\gamma_{ps}^{cl}=2/\iota^2$. For the considered configu-

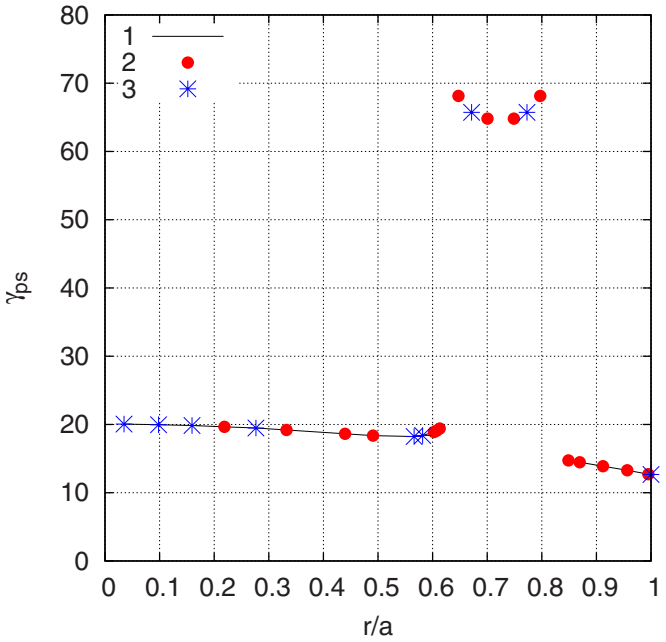

FIG. 6. (Color online) The same as in Fig. 5 for $k_\varphi=0.295$. Enhanced values of γ_{ps} for the region $0.61<r/a<0.85$ correspond to island magnetic surfaces with $\iota=1/3$. The values of r/a for this region are shown schematically.

rations the value of ι is within $0.31<\iota<0.383$ for $k_\varphi=0.295$ and $0.335<\iota<0.422$ for $k_\varphi=0.31$. This leads to values of γ_{ps}^{cl} in the range of $20.81>\gamma_{ps}^{cl}>13.63$ for $k_\varphi=0.295$ and $17.82>\gamma_{ps}^{cl}>11.23$ for $k_\varphi=0.31$. It follows from Figs. 5 and 6 that for the considered magnetic configurations the parameters γ_{ps} are rather close to γ_{ps}^{cl} for the nonisland magnetic surfaces. (For a discussion of results with bad convergence see Sec. IV E.)

C. Calculation of the bootstrap current in the $1/\nu$ regime

In many papers the bootstrap current for the $1/\nu$ regime in stellarators is characterized by a certain geometrical factor denoted below as λ_b. This factor enters into the expression for the bootstrap current as a multiplier which takes into account the magnetic field geometry. In magnetic coordinates such a factor has been studied and calculated for stellarators in a number of papers, e.g., in Refs. 17–19 and Refs. 20 and 21. For the case of real space coordinates the factor λ_b has been obtained in Refs. 22 and 23. In accordance with these references λ_b is determined as a dimensionless quantity by integration along the magnetic field line length, s, and is given as (see also in Ref. 9):

$$\lambda_b=\frac{\langle\lambda_{PS}B^2\rangle}{\langle B^2\rangle}+\lambda_B, \tag{25}$$

with

$$\lambda_{PS}(s)=\frac{2B_0^2}{\langle|\nabla\psi|\rangle}Y_{PS}(s),\quad Y_{PS}(s)=\int_{s_m}^{s}ds'\frac{|\nabla\psi|k_G}{B^2}, \tag{26}$$

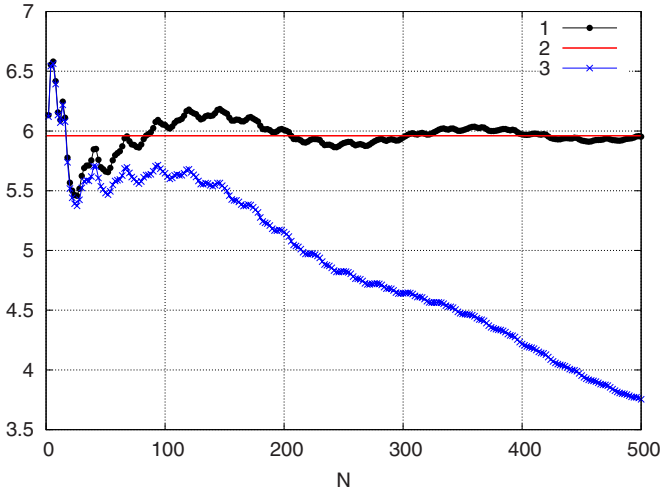

FIG. 7. (Color online) Geometrical factor λ_b, characterizing the bootstrap current, for the same magnetic surface as for Figs. 2–4; 1: evolution of $\lambda_b(L)$ along the magnetic field line, 2: corresponding value of λ_b, 3: evolution of $\lambda_b(L)$ in case of using Eq. (22) for the computation of $\nabla\psi$. N is the number of turns around the main axis of the torus.

$$\lambda_B=\frac{3B_0^2}{8\langle|\nabla\psi|\rangle}\lim_{L\to\infty}\frac{1}{v^3}\int_0^{J_{\perp\min}^{abs}}dJ_\perp J_\perp^2\frac{1}{I_L}\int_{s_m}^{L}ds\frac{|v_\parallel|}{B}Y_B(s), \tag{27}$$

$$Y_B(s)=\int_{s_m}^{s}ds'\frac{B|\nabla\psi|k_G}{|v_\parallel|^3},\quad I_L=\int_{s_m}^{L}ds\frac{|v_\parallel|}{B}, \tag{28}$$

where $v_\parallel^2=v^2-J_\perp B$, $J_\perp=v_\perp^2/B$, $J_{\perp\min}^{abs}=v^2/B_{\max}^{abs}$ corresponds to the trapped-passing boundary, $B_{\max}^{abs}$ is the global maximum of B on the particular magnetic field line, and s_m is the position of this maximum. It follows from the definition of λ_b that this factor depends on the choice of the reference magnetic field B_0. In further computations the different factor λ_{bb}, $\lambda_{bb}=\lambda_b\langle B^2\rangle/B_0^2$, is considered, which is independent from the choice of B_0.

For any magnetic surface a computation of λ_{bb} is performed in three stages. In the first stage, a point corresponding to the global maximum of B, s_m, has to be found by integration of the magnetic field line. In the second stage, the parameter α, described in Sec. II, has to be determined. For this step, s_m is used as initial point for the integration. The geometrical factor λ_b is calculated in the third stage using the integration along the magnetic field line. Simultaneously, $\nabla\psi$ is computed according to Eqs. (1)–(3).

First, computations of λ_{bb} are performed for the magnetic configuration of $k_\varphi=0.31$ for the magnetic field representation with help of toroidal harmonics. Figure 7 shows the evolution of λ_b along the magnetic field line for the same magnetic surface as for Figs. 2–4. The integration starts at $s=s_m$ and the field line is followed 500 turns around the main axis of the torus. It can be clearly seen that $\lambda_b(L)$ (curve 1) is oscillating with decreasing amplitude and finally converges to the value of λ_b (line 2). For comparison curve 3 in Fig. 7 shows $\lambda_b(L)$ where Eq. (22) has been used for the computation of $\nabla\psi$. It is seen that $\lambda_b(L)$ does not converge to any

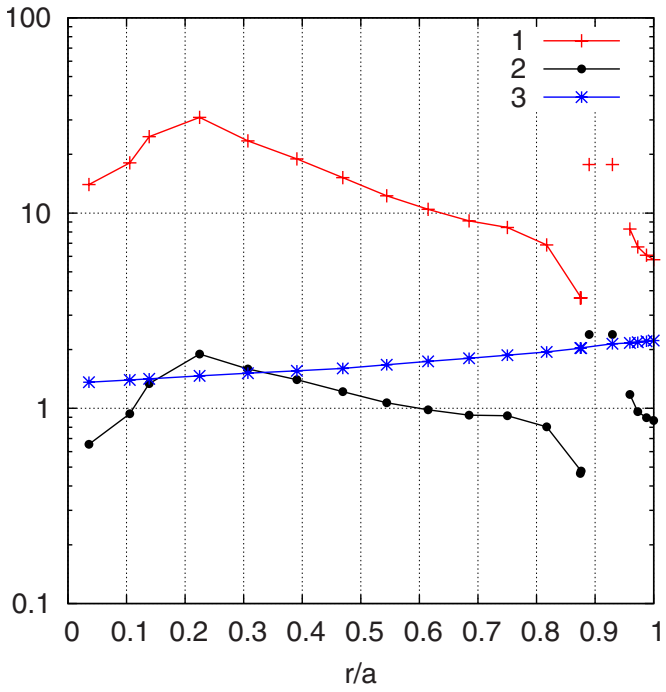

FIG. 8. (Color online) Parameters λ_{bb} (curve 1) and $1/f_c$ (curve 3) for $k_\varphi=0.31$ and with the magnetic field being represented with help of toroidal harmonics. Curve 2 shows a normalized value of λ_{bb}, λ_{bbn}, determined as a ratio of λ_{bb} to the corresponding parameter of an equivalent tokamak; r and a are the same as in Fig. 5. Enhanced values of λ_{bb} and λ_{bbn} for $r/a \approx 0.9$ correspond to island magnetic surfaces with starting points within 144.6 cm $< R_{st} <$ 148.0 cm [see Fig. 1(a)].

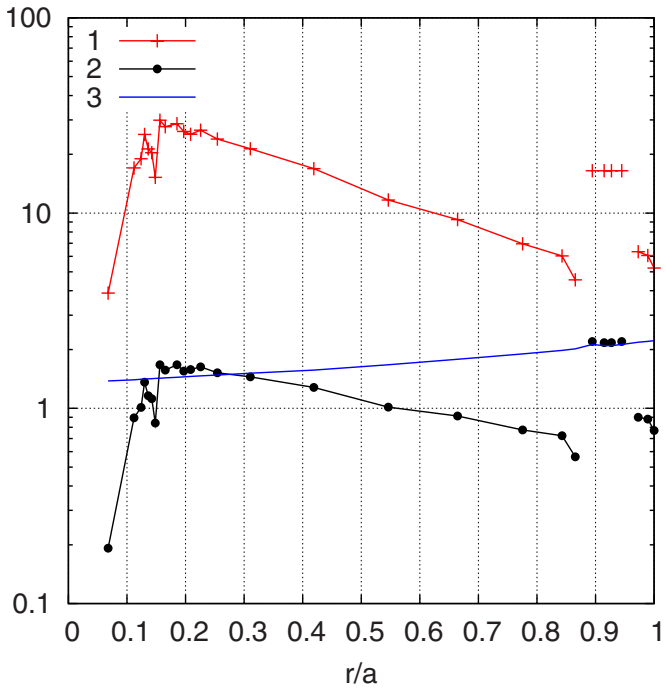

FIG. 9. (Color online) Computational results for the parameters λ_{bb} (curve 1), λ_{bbn} (curve 2) and $1/f_c$ (curve 3) for $k_\varphi=0.31$ in case of using the Biot–Savart code; r and a are the same as in Fig. 5. Enhanced values of λ_{bb} and λ_{bbn} for $r/a \approx 0.9$ correspond to island magnetic surfaces with $\iota=2/5$. The values of r/a for these points are shown schematically.

final value in this case. This phenomenon and the irregularities in the Pfirsch–Schlüter current in Fig. 4 have the same root.

Computational results for λ_{bb} as a function of the mean radius of the magnetic surface are presented in Fig. 8 (see curves 1 and 2). It follows from Ref. 17 that an additional factor enters into the expression of the bootstrap current if the fraction of trapped particles is not very small. This factor is approximately equal to $1/f_c$ with f_c being the fraction of the circulating particles,

$$f_c = \frac{3}{4}\frac{\langle B^2\rangle}{(B_{\max}^{\text{abs}})^2}\int_0^1 \frac{\lambda d\lambda}{\langle (1-\lambda B/B_{\max}^{\text{abs}})^{1/2}\rangle}, \tag{29}$$

with $\lambda = J_\perp B_{\max}^{\text{abs}}/v^2$. In general, this leads to increased values of the general geometrical factor compared to the values of λ_b or λ_{bb}. Computational results for the $1/f_c$ parameter for the same magnetic field parameters as for the λ_{bb} computation are presented in Fig. 8 (curve 3), too. The analogous results for λ_{bb} and $1/f_c$ obtained for the configurations of $k_\varphi=0.31$ and $k_\varphi=0.295$ for the magnetic field computed with the Biot–Savart code are presented in Figs. 9 and 10. Figures 8–10 also show the normalized λ_{bb} value, λ_{bbn}, which is a ratio of λ_{bb} to the corresponding parameter of an equivalent tokamak.

It follows from the computations that for the configuration characterized by $k_\varphi=0.31$ noticeable island magnetic surfaces with $\iota=2/5$ exist near the plasma boundary. A significantly broader (in r/a) island region for $\iota=1/3$ exists for the configuration corresponding to $k_\varphi=0.295$ [see Fig. 1(b)].

The values of λ_{bb} are significantly higher for the indicated island regions than for adjacent nonisland magnetic surfaces. It can be seen that for the considered configurations values of λ_{bbn} for nonisland magnetic surfaces are rather close to unity

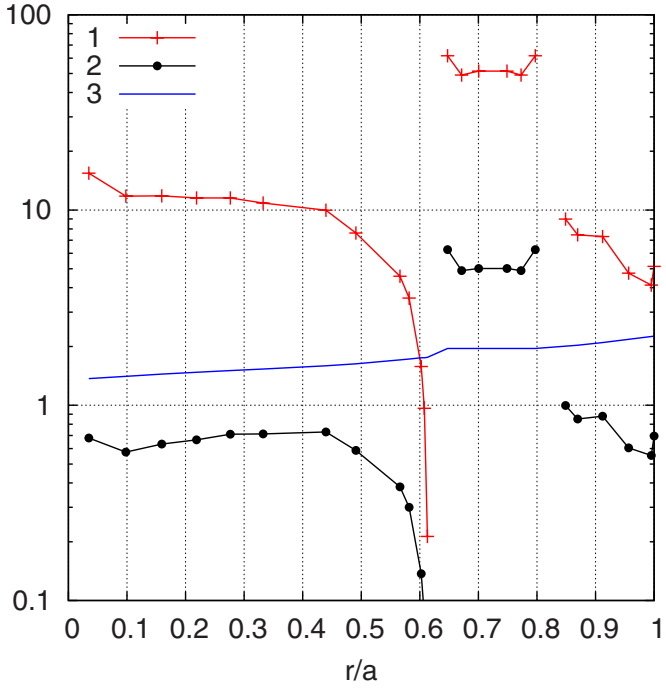

FIG. 10. (Color online) The same as in Fig. 9: for $k_\varphi=0.295$. Enhanced values of λ_{bb} and λ_{bbn} for the region $0.61 < r/a < 0.85$ correspond to island magnetic surfaces with $\iota=1/3$. The values of r/a for this region are shown schematically.

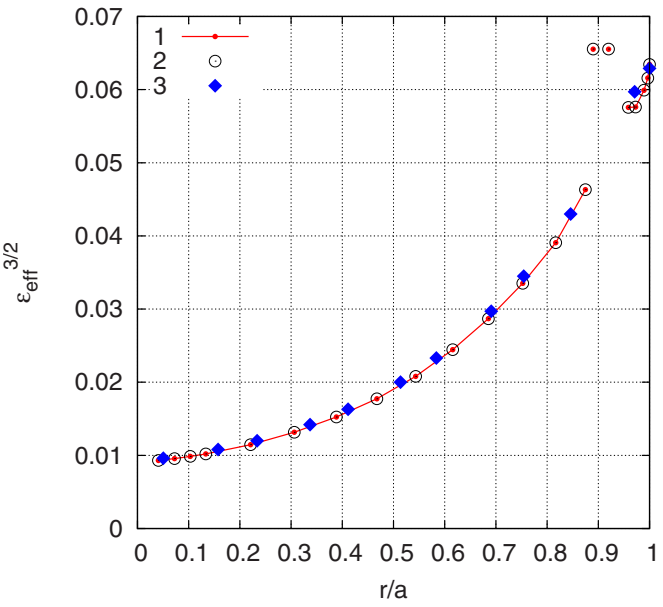

FIG. 11. (Color online) Computational results or $\epsilon_{\text{eff}}^{3/2}$ for k_φ=0.31; 1: for the technique of the $\nabla\psi$ calculation presented in Sec. II, 2: (open circles) for the $\nabla\psi$ calculation using Eq. (22), 3: (rhombi) corresponding results from Ref. 11; r and a are the same as in Fig. 5; enhanced values of $\epsilon_{\text{eff}}^{3/2}$ for $r/a \approx 0.9$ correspond to island magnetic surfaces. Curves 1 and 2 correspond to the magnetic field represented with help of toroidal harmonics.

and, therefore, λ_{bb} is close to the corresponding factor of an equivalent tokamak. Benchmarking the results for λ_{bb} from Fig. 8 (toroidal harmonic functions) and Fig. 9 (Biot–Savart code) one can conclude that these results are in a reasonable agreement.

D. Calculation of the effective ripple

The effective ripple, ϵ_{eff}, is a widely used characteristic quantity for the neoclassical transport in the $1/\nu$ regime for stellarators (see, e.g., in Ref. 15). The quantity $\epsilon_{\text{eff}}^{3/2}$ enters into the $1/\nu$ transport coefficients as a factor which takes into account the magnetic field geometry. Here, $\epsilon_{\text{eff}}^{3/2}$ is calculated using a field line following code based on equations obtained in Ref. 8 for the magnetic configuration of k_φ =0.31 for the magnetic field representation with help of toroidal harmonics. The obtained results for $\epsilon_{\text{eff}}^{3/2}$, expressed as a function of the mean radius of the magnetic surface, are presented in Fig. 11 (curve 1). For comparison, also formula (22) is used for the computation of $\nabla\psi$ which enters into the expression of $\epsilon_{\text{eff}}^{3/2}$. The corresponding results are shown in Fig. 11 (open circles). It can be seen that, practically, these results do not differ from the results when $\nabla\psi$ is calculated using the technique proposed in Sec. II. In Fig. 11 (rhombi) analogous results obtained in Ref. 11 are shown. For this computation the Biot–Savart code has been used and $\nabla\psi$ has been calculated according to Eq. (22). It follows from the comparison that the results of Ref. 11 differ only slightly from those obtained in the present paper. This allows to state that for the $1/\nu$ transport study the calculation of $\nabla\psi$ according to Eq. (22) is quite admissible.

E. Convergence of obtained results

Beside magnetic surfaces with good convergence of the solutions for λ_b and $j_\parallel$ within the used integration interval, there exist magnetic surfaces for which convergence is worse when using the same integration interval. It is found that this phenomenon takes place in the vicinity of resonant (nonisland) magnetic surfaces with a rotational transform ι close to rational. In Figs. 5 and 6 the results are presented for cases of good convergence as well as for cases where convergence is worse. It can be seen in the presented figures that a violation caused by a too short integration interval has no significant influence on the results for γ_{ps} as long as this violation is not too strong.

One has also to keep in mind that in the vicinity of rational magnetic surfaces a reduced convergence of the parameter λ_b can take place even for configurations possessing stellarator symmetry (see Ref. 24). It follows from Ref. 24 that in some cases a substantial increase in the integration interval is necessary to obtain a converged solution for λ_b. Integration intervals of 250–500 turns around the torus can be insufficient for obtaining converged solutions of λ_b, for all magnetic surfaces of the given devices.

V. CONCLUSION

In the proposed technique the magnetic surface gradient, $\nabla\psi$, is represented as a linear combination of gradients of two conveniently chosen, independent, not single valued integrals of the magnetic field line equations. The corresponding coefficients of this combination can be determined using the technique of magnetic field line integration for a sufficiently large integration interval. The requirement that $\nabla\psi$ is single valued should be fulfilled on this interval. The magnetic surface gradient $\nabla\psi$ and associated quantities can be calculated using the obtained coefficients.

To demonstrate its capabilities, this method is applied to the magnetic field of Uragan-2M with broken stellarator symmetry. In Ref. 11 computations of this magnetic field have been performed with help of the Biot–Savart code. This code is used for a part of the computations presented in Sec. IV. In another part of the paper the magnetic field is represented as a superposition of a finite number of toroidal harmonic functions. The chosen number of toroidal harmonics satisfies the condition that the shapes of the magnetic surfaces as well as the rotational transform are in good agreement with those obtained with help of the Biot–Savart code. The usage of expansion in the toroidal harmonic functions allowed to minimize essentially the computer time expenses in those computations which serve to confirm the validity of the approach and the correctness of the general code.

The proposed technique for $\nabla\psi$ computations is applied to U-2M for studies of the $1/\nu$ neoclassical transport as well as the equilibrium currents including the bootstrap current in the $1/\nu$ regime and is accompanied by comparison with the approach of Refs. 11 and 16. The advantage of the new technique is that $\nabla\psi$ can be computed with high accuracy for flux surfaces of magnetic configurations which do not exhibit stellarator symmetry. This has been demonstrated in the pre-

sented comparison. At the same time it is found that the technique applied in Ref. 11 is admissible for the $1/\nu$ transport computation.

ACKNOWLEDGMENTS

This work, supported by the European Communities under the contract of Association between EURATOM and the Austrian Academy of Sciences, was carried out within the framework of the European Fusion Development Agreement. The views and opinions expressed herein do not necessarily reflect those of the European Commission. Additional funding is provided by the Austrian Science Foundation, FWF, under Contract No. P16797-N08.

[1] L. Spitzer, Phys. Fluids **1**, 253 (1958).
[2] M. D. Kruskal and R. M. Kulsrud, Phys. Fluids **1**, 265 (1958).
[3] A. I. Morozov and L. S. Solov'ev, in *Reviews of Plasma Physics*, edited by M. A. Leontovich (Consultants Bureau, New York, 1966), Vol. 2, p. 3; *Voprosy Teorii Plazmy* (Atomizdat, Moscow, 1963), Vol. 2, p. 3, in Russian.
[4] V. D. Shafranov, in *Reviews of Plasma Physics*, edited by M. A. Leontovich (Consultants Bureau, New York, 1966), Vol. 2, p. 103; *Voprosy Teorii Plazmy* (Atomizdat, Moscow, 1963), Vol. 2, p. 92, in Russian.
[5] L. S. Solov'ev and V. D. Shafranov, in *Reviews of Plasma Physics*, edited by M. A. Leontovich (Consultants Bureau, New York, 1970), Vol. 5, p. 1; *Voprosy Teorii Plazmy* (Atomizdat, Moscow, 1967), Vol. 5, p. 3, in Russian.
[6] V. V. Nemov, Nucl. Fusion **28**, 1727 (1988).
[7] V. V. Nemov, Nucl. Fusion **32**, 597 (1992).
[8] V. V. Nemov, S. V. Kasilov, W. Kernbichler, and M. F. Heyn, Phys. Plasmas **6**, 4622 (1999).
[9] V. V. Nemov, V. N. Kalyuzhnyj, S. V. Kasilov, M. Drevlak, J. Nührenberg, W. Kernbichler, A. Reiman, and D. Monticello, Plasma Phys. Controlled Fusion **46**, 179 (2004).
[10] O. S. Pavlichenko for the U-2M group, Plasma Phys. Controlled Fusion **35**, B223 (1993).
[11] V. V. Nemov, V. N. Kalyuzhnyj, S. V. Kasilov, W. Kernbichler, G. G. Lesnyakov, B. Seiwald, and N. T. Besedin, in 34th EPS Conference on Plasma Physics, July 2–6, 2007, Warsaw, Poland, edited by P. Gąsior and J. Wołowski (European Physical Society, Mulhouse, 2007), ECA Vol. 31F, Paper No. P-4.063.
[12] N. T. Besedin, G. G. Lesnyakov, and I. M. Pankratov, Voprosy Atomnoj Nauki i Tekhn., Ser. Termoyadernyj Sintez, Moskva, 1991, Vol. 1, p. 48 (in Russian).
[13] G. G. Lesnyakov, D. D. Pogozhev, Yu. K. Kuznetsov, N. T. Besedin, E. D. Volkov, and O. S. Pavlichenko, in 23rd EPS Conference on Controlled Fusion and Plasma Physics, 24–28 June 1996, Bogolyubov Institute for Theoretical Physics, Kiev, Ukraine, edited by D. Gresillon, A. Sitenko, and A. Zagorodny (European Physical Society, Mulhouse, 1996), ECA Vol. 20C, Part II, p. 547, Report B025.
[14] V. N. Kalyuzhnyj and V. V. Nemov, in "Voprosy atomnoj nauki i tekhniki" Series Termoy-adernyj Sintez, 1985, Vol. 2, p. 35 (in Russian).
[15] G. Grieger, W. Lotz, P. Merkel, J. Nührenberg, J. Sapper, E. Strumberger, H. Wobig, W7-X Team, R. Burhenn, V. Erckmann, U. Gasparino, L. Giannone, H. J. Hartfuss, R. Jaenicke, G. Kühner, H. Ringler, A. Weller, F. Wagner, and W7-AS Team, Phys. Fluids B **4**, 2081 (1992).
[16] H. L. Berk, M. N. Rosenbluth, and J. L. Shohet, Phys. Fluids **26**, 2616 (1983).
[17] K. C. Shaing and J. D. Callen, Phys. Fluids **26**, 3315 (1983).
[18] A. H. Boozer and H. J. Gardner, Phys. Fluids B **2**, 2408 (1990).
[19] N. Nakajima and M. Okamoto, J. Phys. Soc. Jpn. **61**, 833 (1992).
[20] K. Watanabe, N. Nakajima, M. Okamoto, Y. Nakamura, and M. Wakatani, Nucl. Fusion **32**, 1499 (1992).
[21] J. L. Johnson, K. Ichiguchi, Y. Nakamura, M. Okamoto, M. Wakatani, and N. Nakajima, Phys. Plasmas **6**, 2513 (1999).
[22] S. V. Kasilov, V. V. Nemov, W. Kernbichler, and M. F. Heyn, in 27th EPS Conference on Controlled Fusion and Plasma Physics, 12–16 June 2000, Budapest, Hungary, edited by K. Szego, T. N. Todd, and S. Zoletnik (European Physical Society, Mulhouse, 2000), ECA Vol. 24B, p. 668–671, Report P2.066.
[23] W. Kernbichler, V. V. Nemov, S. V. Kasilov, M. F. Heyn, Problems of Atomic Science and Technology, Series: Plasma **6**, 8 (2000).
[24] S. V. Kasilov, V. V. Nemov, W. Kernbichler, and M. F. Heyn, in 28th EPS Conference on Contr. Fusion and Plasma Phys., 18–22 June 2001, Funchal, edited by C. Silva, C. Varandas, and D. Campbell (European Physical Society, Mulhouse, 2001), ECA Vol. 25A, p. 773–776, Report P2.079.